

Design of rubble mound breakwaters

Structural Integrity

by

Hans F. Burcharth

Department of Civil Engineering

Aalborg University, Denmark

Contents	P
1 Geometrical properties and durability of rock materials	4
1.1 Availability	2
1.2 Block weight, size and grading	2
1.3 Block shape	4
1.4 Surface profile	5
1.5 Durability of rock materials	5
2 Structural integrity of concrete armour units	8
2.1 Introduction	8
2.2 Types of loads	9
2.3 Scaling stresses from static and dynamic loads	10
2.4 Determination of stresses from static and dynamic loads	11
2.4.1 Scaled material properties	11
2.4.2 Recording of armour unit movements	12
2.4.3 Load cell technique	13
2.5 Characteristics of stresses from static and dynamic loads in slender armour units	16
2.6 Fatigue	18
2.6.1 Unreinforced concrete	18
2.6.2 Reinforced concrete	22
2.6.3 Implementation of fatigue in the design process	22
2.7 Ultimate impact velocities for concrete armour units	24
2.8 Thermal stresses	25
2.9 Design diagrams for Dolos of different waist ratios	28
3 References	34

1. Geometrical properties and durability of rock materials

1.1 Availability

Rubble mound breakwaters require availability of often very large quantities of rock materials of various gradings and qualities.

Because natural stones are seldom available in sufficient quantities and sizes the materials must in most cases be supplied from quarries. The output from a quarry in terms of sizes and shapes is, however, not only dependent on the applied blasting technique but to a large extent on the type of rock and the degree of weathering. This creates very different discontinuity patterns which again determine the size and shape of the blocks. Also the strength and durability of the rock material are functions of rock type and the degree of weathering. Thus it is important to establish the availability and quality of rock material before completion of a breakwater design for a particular location. If this is not possible then design changes are to be foreseen during the construction stage.

Anyway, it is seldom that a fair amount of rocks of mass larger than 10-15 t can be produced, even in good quality quarries. If heavier blocks are needed concrete armour units or vertical structures must be considered.

1.2 Block weight, size and grading

A sample of quarry blocks will cover a range of block weights (or masses). The cumulative distribution of block weights is the basis for the definition of characteristic block weights, sizes and gradings, Fig. 1.1.

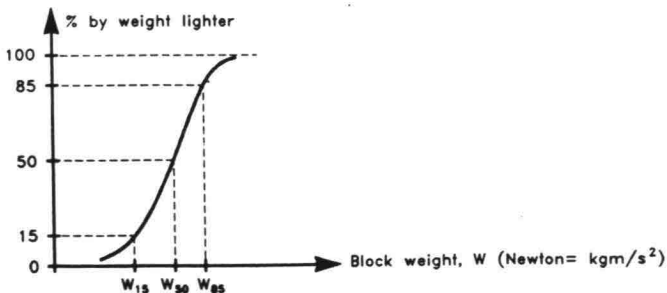


Fig. 1.1. Illustration of cumulative block weight distribution curve.

The equivalent cube length D_{n50} used in armour layer stability formulae is defined as

$$D_{n50} = \left(\frac{W_{50}}{\rho g} \right)^{1/3} \tag{1.1}$$

where W_{50} is the median weight and ρ is the mass density of the block. The equivalent sphere diameter is $D_s = 1.24 D_n$.

In case of smaller blocks and finer stone materials it is more convenient to use sieve analyses (square opening) instead of block weight as the basis for definition of characteristic values, Fig. 1.2.

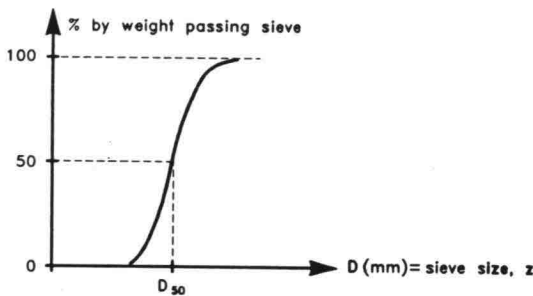


Fig. 1.2. Illustration of cumulative sieve diameter distribution curve.

The ratio between the equivalent cube length, D_{n50} and the median sieve size, D_{50} , varies. However, a typical ratio is $D_{n50}/D_n = 0.84$.

As an indicator of the gradation (grading width) is often used the ratio, $D_{85}/D_{15} = (W_{85}/W_{15})^{1/3}$ or W_{85}/W_{15} .

In breakwater engineering the following classes are often used, Table 1.1.

Table 1.1. Conventional gradings and their application.

Gradation	D_{85}/D_{15}	Application (conventional)
Narrow (single size)	≤ 1.5	Armour, berms, underlayers
Medium	1.5 – 2.5	Underlayers, filter layers, (berms, armour)
Wide (quarry run)	2.5 – 5 (or more)	Core material






1.3 Block shape

The hydraulic stability of rock armour depends on the shape of the armour. However, no generally accepted standard for characterization of the block shape exists. Several systems for defining the gross shape using axial dimensions have been proposed. The system described here makes use of the following definitions:

- ℓ : maximum axial length given by the maximum distance between two points on the stone
- d : thickness given by the minimum distance between two parallel straight lines through which the stones can just pass
- z : sieve size, i.e. width of the smallest square hole that a stone can pass through with optimum orientation

The d/z ratio (generally in the order of 0.75) can distinguish tabular from elongate stones. This distinction is of no great significance as the aspect ratio ℓ/d alone can provide the essential degree of departure from the equant form which gives optimum hydraulic stability for armour made of randomly placed blocks. Table 1.2 shows visually based definition of shape classes.

Table 1.2. Definition of shape classes for blocks.

	Angular Stones with surface bounded by sharp edges and corners			Rounded Most corners and edges show clear signs of wear and crushing	
Shape class	Elongate + tabular	Irregular	Equant	Semiround	Very round
					
Typical sources	Columnar joints, basalts, bedded sedimentary metamorphic rock	Massive sediment and igneous rocks, some metamorphic rocks	Massive sediment and igneous rocks	Softer sedimentary rocks rounded during wear	Dredged sea stones, glacial and river boulders
Mean aspect Ratio ℓ/d	> 3.0	2.0-3.0	1.5-2.0	1.5-3.0	1.0-2.5

The aspect ratio ℓ/d is generally in the order of 2.0-2.5 ($\ell/d = 1.73$ for a cube). For armour stones gradings it is in most cases prescribed that only a limited proportion, e.g. 30-50%, of the blocks must have a ℓ/d ratio larger than 2 and no ℓ/d ratio larger than 3.

In some cases elongate quarry stones placed with the long axis perpendicular to the slope are used as main armour. By using this kind of special placement pattern a higher hydraulic stability of the armour can be achieved, but will result in a more sudden (brittle) failure of overloaded.

1.4 Surface profile

There is no standard definition of the surface profile of a rock armoured slope. Nor is there a standard method for the measurement of the surface. However, it is probably generally agreed that a reasonably easy and meaningful way of determine *the surface* is by using a staff or a sounding line with a spherical end of diameter $D_{n50}/2$ to measure levels spaced approximately D_{n50} . This technique ensures that the peaks and troughs are somewhat smoothed out and defines a surface which fits the visually defined surface quite well.

1.5 Durability of rock materials

The hydraulic stability of rock materials in armour layers depends mainly on the weight and density of the stones. Also the shape and surface roughness are of importance for armour stones. For underlayers mainly the size of the stones is of importance. As a consequence it is necessary to evaluate the ability of the stone material to resist degradation in terms of disintegration and abrasion, related to the environmental impacts and the service life of the structure.

The durability depends first of all on the *type of rock* and the stage of the *in situ chemical and physical weathering*.

Also *production and handling* can influence the long term integrity of the armour stones because blasting, crane, dozer and dumper handling can induce fissures which at a later stage cause disintegrations. Underlayer stones can be weakened in a similar way by crushing and screening processes.

Deterioration during *service life* takes place due to *physical weathering* (e.g. temperature induces stresses including freeze-thaw, wetting-drying, salt crystallization) which leads to disintegration, surface spalling and rounding and consequently weight loss. Also *abrasion* due to wave induced action of sand and gravel as well as the grinding-impacting effect of moving armour stones causes weight loss and rounding. Berm breakwaters designed for movement of the armour stones (dynamic stability) are vulnerable to the last mentioned effect.

Evaluation of the durability is first of all based on *visual inspection* in order to identify the type of rock, the degree of weathering and the discontinuity patterns. Table 1.3 gives some relevant intrinsic characteristics of the most important types

of unweathered rock used in the marine environment.

The rock should not be more than slightly weathered, i.e. the rock might be discoloured but no proportion should be decomposed/disintegrated to a soil.

The discontinuity patterns determine the maximum size and the shape of the quarry stones. Thus the discontinuity spacing must be evaluated on the basis of specified block sizes.

Table 1.3. Typical intrinsic characteristics of unweathered types of rock used in the marine environment.

Rock type	Density (t/m ³)	Water absorption (%)	Discontinuity (joint) spacing (m)	Block shape when quarried	Suitability **)
<i>Igneous</i>					
Granite	2.5 - 2.8	2.0 - 0.2	0.5 - 10	equant	very good
Gabbro	2.8 - 3.2	2.5 - 0.2	0.5 - 10	—	—
Rhyolite	2.3 - 2.8	5 - 0.2	0.1 - 2	angular/equant	good, but often small block
Andesite	2.4 - 3.0	10 - 0.2	0.2 - 2	—	good, but often small block
Basalt	2.5 - 3.1	1.0 - 0.1	0.2 - 5	—	very good, but often small block
<i>Sedimentary</i>					
Quartzite	2.6 - 2.8	0.5 - 0.1	0.1 - 5*)	often tabular	often poor abrasion resistance
Sandstone	2.3 - 2.8	15 - 1.0	0.1 - 10*)	angular, but can be tabular	often too soft
Siltstone	2.3 - 2.8	10 - 1.0	0.05 - 1*)	tabular	often too soft and very small sized
Limestone	2.3 - 2.7	5 - 0.2	0.5 - 1*)	angular, but can be tabular	often too soft and very small sized
<i>Metamorphic</i>					
Slate	2.7 - 2.8	5 - 0.5	< 0.1	tabular	small sized
Phyllite	2.3 - 2.7	6 - 0.2	< 0.2	elongate	small, often soft
Schist	2.7 - 3.2	5 - 0.4	0.01 - 1	elongate	small sized, can be soft
Gneiss	2.6 - 2.8	1.5 - 0.5	0.5 - 10	equant	good

*) Bed thickness

***) See also Table 1.4.

The rock *density* is generally a good indicator of durability ($> 2.8t/m^3$: very good, $< 2.3t/m^3$: poor). A very important overall indicator is the *water absorption* ($< 0.5\%$: very good, $> 6\%$ very poor). Table 1.4 gives typical parameter limits for standard application of rock materials in breakwaters.

Table 1.4. *Typical parameter limits for standard application of rock materials in breakwaters.*

	Armour	Underlayers/filters	Core
Discontinuity spacing	$\geq 1m^{*1}$	$\geq 0.5m^{*1}$	$\geq 0.2m$
Density	$\geq 2.6t/m^3$	$\geq 2.6t/m^3$	$\geq 2.3t/m^3$
Water absorption	$< 2\%$	$< 2.5\%$	$< 3\%$

*1) depends on specified sizes of the blocks.

For more detailed information on rock properties reference is made to CIRIA-CUR (1991).

Further evaluation of the durability is based on results from various tests such as magnesium sulphate soundness tests (important for porous sedimentary rocks for use in hot dry climate), freeze-thaw tests (important in cold-regions), mill abrasion resistance tests (restricted to small samples) and drop tests (to indicate impact resistance to breakage of large blocks). Detailed descriptions of durability tests are given in CIRIA-CUR, 1991.

2. Structural integrity of concrete armour units

2.1 Introduction

The various types of concrete armour units might be divided into the following categories related to the structural strength:

- Massive or blocky* (e.g. cubes incl. Antifer type, parallelepiped block)
- Bulky* (e.g. grooved cube with hole, Seabee, Accropode, Haro, Dolos with large waist ratios)
- Slender* (e.g. Tetrapod, Dolos with smaller waist ratios)
- Multi-hole cubes* (e.g. Shed, Cob)

The units are generally made of conventional unreinforced concrete except the multi-hole cubes where fibre reinforcement is used.

For slender units as Dolos with small waist ratios various types of high-strength concrete and reinforcement (conventional bars, prestressing, fibres, scrap iron, steel profiles) have been considered, but only used in few cases as it generally seems to be less cost effective.

The hydraulic stability of armour layers is hampered if the armour units disintegrate because this causes reduction of the stabilizing gravitational force and possible interlocking effects. Moreover, broken armour unit pieces can be thrown around by wave action and thereby trigger accelerated breakage. In order to prevent this it is necessary to ensure structural integrity of the armour units.

Unreinforced concrete is a brittle material with a low *tensile strength*, S_T , in the order of 1.5-3 MPa (N/mm^2) and a *compressive strength*, S_C , which is one order of magnitude larger than S_T . Consequently, the reason for crack formation and breakage is nearly always that the load induced *tensile stresses*, σ_T , exceeds S_T . The magnitude of S_T is therefore of much more interest than S_C , a fact that should be reflected in the specifications for armour unit concretes. It is important to notice that S_T decreases with repeated load due to *fatigue* effects.

The different categories of units are not equally sensitive to breakage. *Slender units* are the most vulnerable because the limited cross sectional areas give rise to relatively large tensile stresses. Many recent failures of breakwaters armoured with Tetrapods and Dolosse were caused by breakage of the units before the hydraulic stability of intact units expired. These accidents could have been avoided if design diagrams for structural integrity had been available at the time of design. The situation at present is that structural integrity diagrams are available only for Dolos (Burcharth et al. 1988, 1991, 1992), cf. section 2.9. Dutch research (Ligteringen et al. 1990) and research of the Franzius Institute, Univ. of Hannover (Bürger et

al. 1990) might result in design diagrams for Tetrapods.

Massive units will generally have the smallest tensile stresses due to the large cross sectional areas. However, breakage can take place if the units are impacting due to application of less restrictive hydraulic stability criteria and if the concrete quality is poor in terms of a low S_T . The last point is related mainly to larger units where temperature differences during the hardening process can create tensile stresses which exceed the strength of the weak young concrete, thus resulting in micro-cracking of the material (thermal cracking). If massive units are made of good quality concrete and not damaged during handling, and designed for marginal displacements, there will be no breakage problems. With the same precautions this statement holds also for the *bulky units*.

No structural integrity design diagrams exist for the massive units. Available is only some information on maximum impact speeds which is useful for the assessment of hydraulic stability design criteria, and handling and construction methods.

2.2 Types of loads

The different types of loads on armour units and their origins are listed in Table 2.1.

Table 2.1. Types and origins of loads on armour units. Burcharth, 1983.

TYPES	ORIGIN OF LOADS	
Static		<ul style="list-style-type: none"> Weight of units Prestressing of units due to wedge effect and arching caused by movement under dynamic loads
Dynamic	Pulsating	<ul style="list-style-type: none"> Gradually varying wave forces Earthquake
	Impact	<ul style="list-style-type: none"> Collisions between units when rocking or rolling, collision with underlayers or other structural parts Missiles of broken units Collisions during handling, transport and placing High-frequency wave slamming
Abrasion		<ul style="list-style-type: none"> Impacts of sand, shingle etc. in suspension
Thermal		<ul style="list-style-type: none"> Temperature differences during the hardening (setting) process after casting Freeze - thaw
Chemical		<ul style="list-style-type: none"> Alkali-silica and sulphate reactions, etc. Corrosion of steel reinforcement

Static, pulsating and impact loads are critical for slender units whereas impact loads and thermal loads are more important for massive and bulky units. However, very few of the loads and related stresses or deteriorational effects can be quantified.

Fig. 2.1 illustrates a typical stress signal from a point of the surface of a slender/bulky type of armour unit exposed to waves. The different character of the contributions from impact, pulsating and static loads are clearly seen.

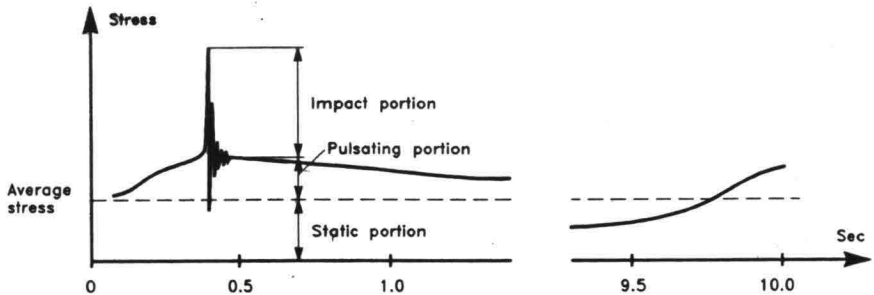


Fig. 2.1. Illustration of stress signal from prototype armour unit.

2.3 Scaling stresses from static and dynamic loads

The various methods for calculation or measurement of stresses from static and dynamic loads are discussed by Burcharth et al. 1991. Generally, stress determination is a very difficult task because of the stochastic nature of the wave loads, the complex shape of the units and their random placement. One of the main problems is that the two main failure modes for armour, namely displacements (hydraulic instability) and breakage (structural instability) are interrelated and must be studied together. However, while the first one can be studied conveniently in small Froude scale models the second one cannot because the stress levels are too small to cause any breakage of the model armour units when made of mortar or other conventional model materials. In order to understand the problem the model scales for stresses, σ , caused by static, pulsating and impact loads in a Froude model are summarized as follows:

$$\lambda_{\sigma_{Static}} = \lambda_{\sigma_{Pulsating}} = \lambda_{\rho_w} \lambda_L \quad (2.1)$$

$$\lambda_{\sigma_{Impact}} = (\lambda_{\rho_A} \lambda_{E_A} \lambda_L)^{0.5} \quad (2.2)$$

E_A is the modulus of elasticity of the armour unit concrete and L is a characteristic characteristic length. ρ_w and ρ_A are the mass densities of water and armour units,

respectively.

It is seen from eq (2.1) and (2.2) that the scaling laws are different which means that in general the two categories of stresses must be identified and measured separately in the model in order to produce a correct up-scaling of the total stresses to prototype conditions.

Moreover, it is seen that static and pulsating stresses scale linearly with the length scale (e.g. D_n) whereas the impact stresses scale with the square root of the length scale. This means that the static stresses grow much more rapidly with the size of the armour than the impact stresses. Consequently, the static stresses are often dominating in the very large slender armour units.

2.4 Determination of stresses from static and dynamic loads

2.4.1 Scaled material properties

Because breakage of a larger proportion (say > 10%) of the armour units will accelerate the hydraulic instability it would be ideal to test a design in a hydraulic model with armour units with correctly scaled material properties. Such a model will exhibit a true picture of prototype damage.

The scaling conditions for material stress and strength would be:

$$\lambda_{\sigma_{Static}} = \lambda_{\sigma_{Impact}} = \lambda_{S_C} = \lambda_{S_T} \quad , \quad (2.3)$$

where λ_{S_C} and λ_{S_T} are the scales of compressive and tensile strengths, respectively.

The scaling conditions for the hydraulic stability correspond to the Froude scaling which implies

$$\lambda_{\Delta} = 1 \quad \text{where} \quad \Delta = \frac{\rho_A}{\rho_W} - 1 \quad , \quad (2.4)$$

i.e. constant ratio of ρ_A/ρ_W in model or prototype or

$$\lambda_{\rho_A} = \lambda_{\rho_W} = \lambda_{\rho} \quad (2.5)$$

Hence we obtain from eq (2.1) - (2.5)

$$\lambda_{E_A} = \lambda_L \lambda_{\rho} \quad (2.6)$$

Moreover, the resistance of the material to crack propagation (fracture toughness) in terms of the critical stress intensity factor K_{1C} , should be scaled correctly, Burcharth (1981). For a given type of crack (surface or internal) $K_{1C} = f \sigma \sqrt{\pi d}$, where the factor, f , depends on the type of crack, σ is the tensile stress σ_T at some distance from the crack and d is the depth or diameter of the crack. Thus for a

given type of crack we get the scaling law

$$\lambda_{K_{1C}} = \lambda_\rho \lambda_L^{3/2} \quad (2.7)$$

If we consider a typical prototype concrete (subindex P) with $E_{A,P} = 4 \cdot 10^4 \text{ N/mm}^2$, $S_{C,P} = 30 \text{ N/mm}^2$, $S_{T,P} = 3 \text{ N/mm}^2$, $\rho_{A,P} = 2.35 \text{ t/m}^3$ $K_{1C} \simeq 30 \text{ N/mm}^{3/2}$ (static value), and a hydraulic model length scale $\lambda_L = \frac{1}{36}$, and $\lambda_\rho = 0.98$ then the following model armour unit material properties (subindex M) are requested:

$$E_{A,M} = 0.11 \cdot 10^4 \text{ N/mm}^2$$

$$S_{C,M} = 0.82 \cdot 10^4 \text{ N/mm}^2$$

$$S_{T,M} = 0.082 \cdot 10^4 \text{ N/mm}^2$$

$$\rho_{A,M} = 2.30 \text{ t/m}^3$$

$$K_{1C} = 0.14 \text{ N/mm}^{3/2}$$

It is extremely difficult to produce such a material when the density should be kept almost as high as for normal concrete. Timco (1981) had some success in producing a material which almost fulfilled the criteria except for $E_{A,M}$, which was much too high. A practical problem was the low surface resistance of the material which caused a rapid rounding (abrasion) of the armour units. Timco et al. (1983) describe model tests with the use of the scaled material.

A drawback of the method of scaled material is that a new material must be produced for each length scale, cf. eq (2.6). Another is, that no general information on stresses is obtained except the information on the exceedence of the strength level when the units break.

2.4.2 Recording of armour unit movements

Impact stresses might be estimated on the basis of impact velocities determined in hydraulic model by cine/video technique or by accelerometers installed inside the units. The methods involve many problems. Cine/video techniques generally fail to give information in the splash zone. Moreover, because it is almost impossible to calculate stresses from information only of the impact speed of the impinging body it is necessary to calibrate the stress calculations method against known behaviour of prototype armour. Van der Meer et al. (1991) describe a Dutch CUR project where the probability density functions of impact speeds of cubes and Tetrapods were studied. Pulsating and static stresses, which are of great importance for large slender units, cannot be determined by the described method.

Surface or bar mounted strain gauges

A direct way of determining stresses is to use strain gauges mounted directly on the concrete surface or on bars cast in the concrete close to the surface where

the largest strains occur. The limitation of the method is the small strain values in case of small units exposed only to static and pulsating loads. The method cannot be applied even to large model armour units, say of 50 kg, unless a very sophisticated strain gauge technique is used. Strain gauge mounted bars have been used successfully in 38 tons prototype Dolosse in the CERC Crescent City research project, Howell (1985, 1988).

2.4.3 Load cell technique

Load cells have been used to study the resulting wave induced flow forces on armour units for quite some years, Sandstrom (1974). Few years later the load cell technique was used to study the stresses in slender/bulky types of armour units, Delft Hydraulics (1980), Scott et al. (1986), Aalborg University (1987), Markle (1990), Bürger et al. (1990). The method consists of inserting a load cell able to record the component forces and moments in the critical sections of the armour units. The critical sections are those where the largest stresses and, consequently, the fractures generally occur. Fig. 2.2 illustrates the critical sections, the related component forces and moments, and a load cell by which the components can be recorded.

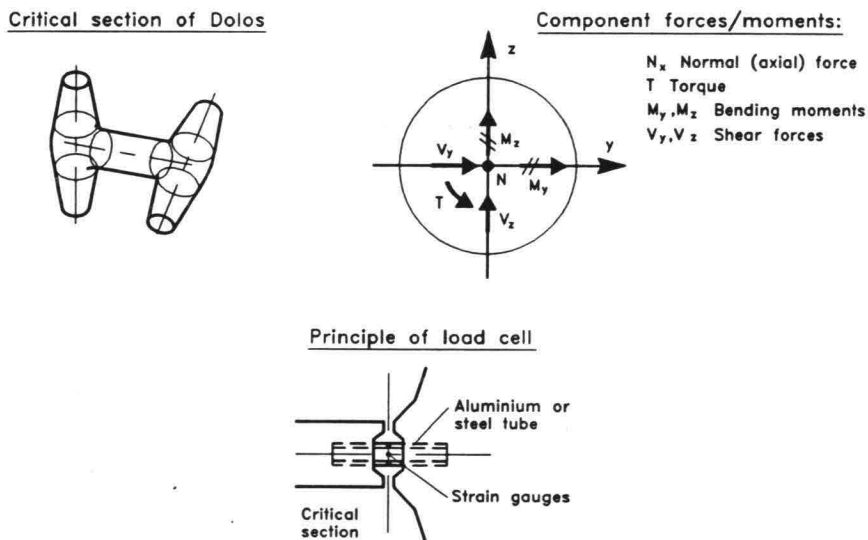


Fig. 2.2. Illustration of critical sections and related component forces and moments.

If beam theory is assumed valid and the cross sections are circular or almost circular then the maximum principal tensile stress at the surface, σ_T , where the most critical

stress conditions are known to occur, can be estimated from the cross sectional component forces and moments as follows:

$$\sigma_T = \frac{\sigma_{xx}}{2} + \sqrt{\left(\frac{\sigma_{xx}}{2}\right)^2 + \sigma_{x\alpha}^2} \quad (2.8)$$

where, cf. Fig. 2.3

$$\sigma_{xx} = \frac{4 N_x}{\pi d^2} + \frac{d}{2I} (M_y \sin\theta - M_z \cos\theta) \quad (2.9)$$

$$\sigma_{x\alpha} = \frac{T d}{4I} + \frac{(1 + 2\nu) d^2}{16(1 + \nu) I} (V_z \cos\theta - V_y \sin\theta) \quad (2.10)$$

d is the diameter of the cross section, $I = (\pi/64) d^4$ is the modulus of the section and ν is Poisson's ratio.

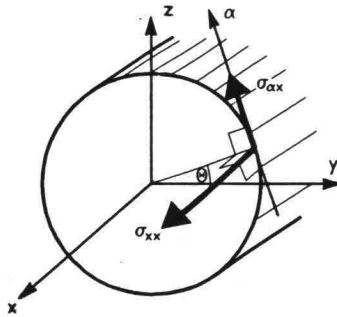


Fig. 2.3. Stress components at the surface.

Failure is usually taken as the appearance of the first crack at the surface, i.e.

$$\sigma_T \geq S_T \quad (\text{failure criterion}) \quad (2.11)$$

where S_T is the tensile strength of the concrete (1.5 - 3 N/mm² for conventional armour unit concrete).

Burcharth et al. (1988) used a load cell with four rosette strain gauges each with three gauges (12 gauges in total) in order to record all six component forces/moments per cross section in 200 kg Dolos of which four sections were instrumented, Fig. 2.4. Markle (1990) developed a very sensitive small scale load cell able to record with good accuracy the most important components (bending moments and torque) in one section of a 200 g Dolos, Fig. 2.5. Small scale load cell technique is of great importance because design diagrams must be based on a very large number of parametric hydraulic model tests which - for economical reasons - cannot be performed at larger scales.

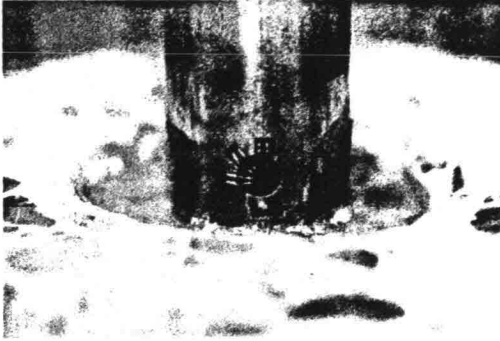


Fig. 2.4. Photo of the Aalborg University six component load cell (200 kg Dolos).

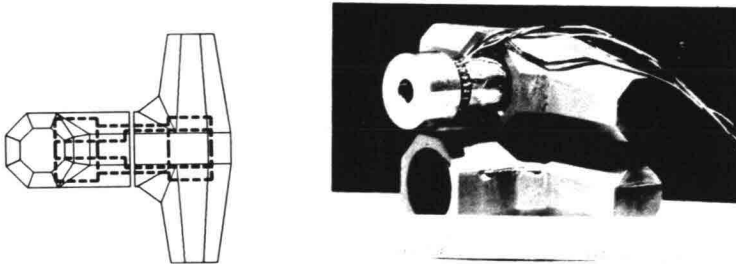


Fig. 2.5. The CERC three component load cell (200 g Dolos).

One of the most difficult problems to overcome when applying the load cell technique is that the impact response is not reproduced to scale because the presence of the load cell makes the dynamic material properties different from those of the monolithic prototype unit. Burcharth et al. (1990) presented a method to overcome the problem by determining an apparent modulus of elasticity of the instrumented units by calibration against prototype impact test results. The design diagrams for Dolos presented in section 2.9 are based on this technique.

2.5 Characteristics of stresses from static and dynamic loads in slender armour units

The following discussion of the characteristics of static and dynamic stresses is based mainly on the results from experiments with load cell instrumented Dolosse (waist ratio 0.32 - 0.42) at Aalborg University. It is believed that for slope in the range 1 : 1.4 - 1 : 2 the following characterizations are valid for all types of slender-bulky units where bending moments/torsion cause the maximum stresses.

- a. The surface roughness affects the static stresses due to its influence on the wedging. Consequently, model armour units should have correct surface roughness.
- b. The distribution of the maximum tensile stress peak values caused by static and pulsating loads follows the log-normal distribution, i.e. $\ln(\sigma_{Static+Pulsating}/\rho g D_n)$ is normally distributed with average, $\mu = a + b H_s/D_n$ and standard deviation, $std = c - d H_s/D_n$, where a , b , c and d are coefficients.

The bottom layer units experience both larger static and pulsating stresses than the top layer units.

The pulsating stresses increase almost linearly with the significant wave height.

The short term distribution of the pulsating stresses, i.e. for constant significant wave height, follows the Rayleigh distribution.

- c. The distribution of impact stress peak values of significance follows a truncated log-normal distribution.
- d. The relative importance of static, pulsating and impact stresses depends on the type and size of the units, the slope angle, the position on the slope and the wave characteristics.

The variation with the position within the critical part of the slope (i.e. $MSW \pm H_s$) is not so large and cannot motivate changes in the strength of the units. Consequently, no distinction with respect to position is made.

Table 2.2 indicates typical ratios between the various types of stresses for slender and bulky Dolosse on slope 1 : 1.5.

Table 2.2. Typical ratios of 2% exceedence probability values of static, pulsating and impact stresses for slender and bulky Dolosse on slope 1 : 1.5.

Waist ratio	Dolos mass (t)	$N_s = \frac{H}{\Delta D_n}$	$\sigma_{Static} : \sigma_{Static+Pulsating} : \sigma_{Static+Pulsating+Impact}$		
0.325	10	0.9	1	1.2	1.2
		1.8	1	1.4	1.4
		2.6	1	1.5	1.9
	20	0.9	1	1.2	1.2
		1.8	1	1.4	1.4
		2.6	1	1.5	1.8
	50	0.9	1	1.2	1.2
		1.8	1	1.4	1.4
		2.6	1	1.5	1.5
0.42	10	0.9	1	1.2	1.2
		1.8	1	1.4	1.4
		2.6	1	1.6	3.6
	20	0.9	1	1.2	1.2
		1.8	1	1.4	1.4
		2.6	1	1.6	3.4
	50	0.9	1	1.2	1.2
		1.8	1	1.4	1.4
		2.6	1	1.6	2.9

The ratios corresponding to 1-5 % exceedence probability are very close to those shown in Table 2.2.

The variation with the slope angle is not known in general. However, because static stresses show only small variations in the slope range 1 : 1.4 to 1 : 2 it is assumed that the stress ratios given in Table 2.2 are typical for this range of slopes. On the other hand the ratios are probably not valid for very steep slopes as it is known that the static stresses can be up to 100% larger for a 1 : 1 slope than for a 1 : 1.5 slope.

For flat slopes of app. 1 : 4 to 1 : 6 it was found from the Crescent City prototype study with 38 t instrumented Dolosse, Howell et al. (1990), that the ratio of the 10 % exceedence probability stress values, $\sigma_{Static} : \sigma_{pulsating}$, was app. 1 : 0.12 for $N_s = 1.2 - 1.4$. No impact stresses were recorded in this study, probably due to the small N_s -values, cf. also the figures given in Table 2.2.

2.6 Fatigue

The strength of concrete reduces with the number of stress cycles. Each stress cycle larger than a certain range will cause partial fracture in some parts of the material matrix resulting in a low strength. Repeated loads cause an accumulative effect which might result in macro cracks and, consequently, breakage of the structural element.

The number of stress cycles caused by wave action will be in order of 200 million during 50 years' structural life in the North Atlantic area. About 10 million will be caused by larger storm waves. In subtropical and tropical areas the number is generally one or two orders of magnitude less.

Since 1903 it has been known that concrete shows significant fatigue. Considering the high stress levels in some of the slender types of armour units it is important to evaluate the fatigue effect. Reference is made to Burcharth (1984) for a more detailed discussion.

2.6.1 Unreinforced concrete

Fig. 2.6 shows results from uniaxial fatigue tests with small specimens presented in a so-called Wöhler diagram.

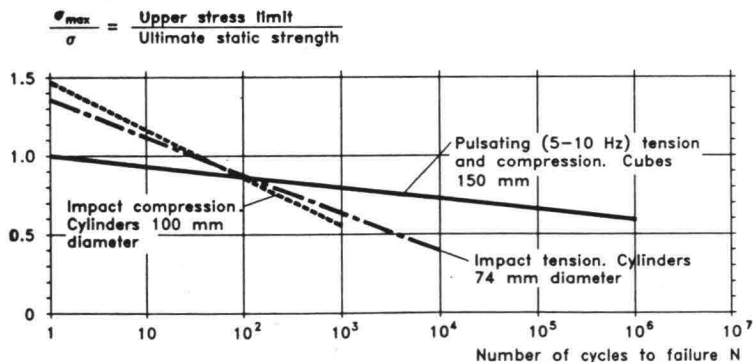


Fig. 2.6. Fatigue. Uniaxial impact and pulsating loading with zero mean. Small unreinforced specimens. Tefers et al. (1979), Fagerlund et al. (1979), Zielinski et al. (1981).

Fig. 2.7 shows fatigue results for 25 kg model Dolosse of 300 mm height exposed to a pulsating load which created mainly uniaxial tensile stresses in the critical section.

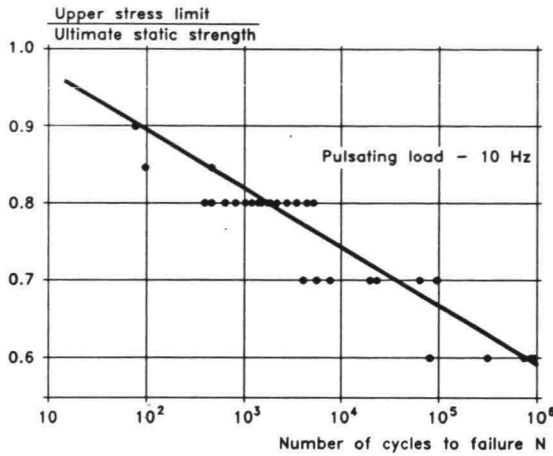


Fig. 2.7. Fatigue. Uniaxial pulsating tension loading with zero mean. Unreinforced model Dolosse of 300 mm height. Tait et al. (1980).

Burcharth (1984) performed fatigue tests with 200 kg Dolosse of 790 mm height exposed to solid impact loads which created flexural stresses in the critical section in order to simulate prototype conditions where the dominating stresses are known to be flexural stresses. The rather large size of Dolosse was chosen in order to use real concretes with aggregate sizes of up to 16 mm and 32 mm. Both unreinforced and steel fibre reinforced concretes were used. The units were supported by a rigid concrete base. Fig. 2.8 shows the results for unreinforced concrete.

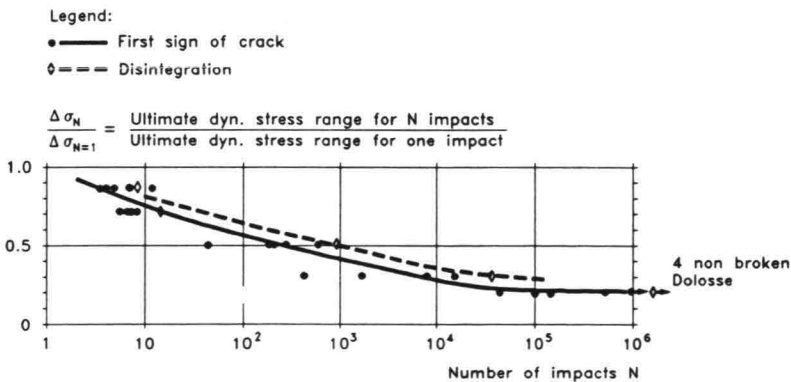


Fig. 2.8. Fatigue due to solid body impact loading of rigidly supported 200 kg unreinforced Dolosse, causing flexural stresses with zero mean. Burcharth (1984).

Note that the ordinate represents the ratio between two dynamic stresses, namely the ultimate dynamic stress range for N impacts over the same quantity for one impact, $N = 1$. In conventional Wöhler diagrams the denominator is the static strength (cf. Figs. 2.6 and 2.8), but the presentation in Fig. 2.8 demonstrates the fatigue effect more clearly.

The full line corresponds to the first sign of crack, thus representing the design graph. The dotted line shows the state of disintegration. No sign of damage or indentation of the impacted Dolos-surfaces were seen in the test series with unreinforced concrete. Burcharth (1984) showed that the results given in the figures above can be presented with good accuracy by only two design graphs, one for pulsating loads and one for solid body impact loads for rigidly supported units, Fig. 2.9. The graphs cover both uniaxial and flexural stress conditions.

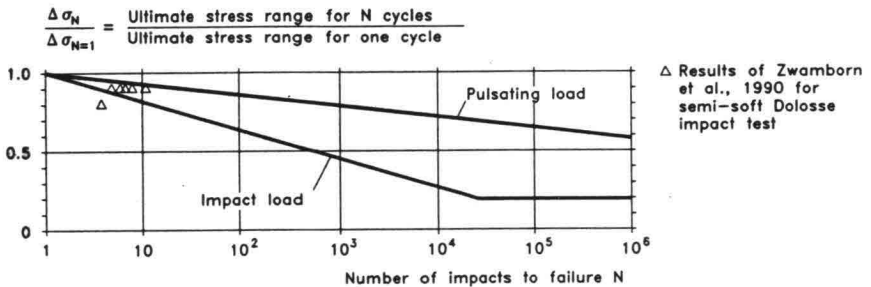


Fig. 2.9. Proposal for universal fatigue curves for conventional unreinforced concrete exposed to uniaxial and flexural stress conditions with zero mean stress. Burcharth (1984).

Zwamborn et al. (1990) performed drop tests with prototype Dolosse on a horizontal underlayer of quarry rock. This relatively soft base creates a milder dynamic response than the solid rigid concrete base used by Burcharth. As seen from Fig. 2.9 Zwamborn's data are, as expected, in between the two curves which might be regarded as upper and lower limits for the fatigue effect.

For practical use of Fig. 2.9 it should be noted that the *ultimate impact load strength* for one stress cycle is in the order of 1.4 and 1.5 times the *ultimate pulsating load strength* in the case of uniaxial tension and compression, respectively, cf. Fig. 2.6. For flexural stresses a factor of approximately 1.4 should be applied. The ultimate pulsating load strength properties for one cycle can be taken equal to those found for static load conditions.

Fatigue tests with prototype unreinforced cubes have been performed by Silva (1983) who conducted solid body impact tests by letting cubes of equal size move on small railway cars with equal speed against each other. Fig. 2.10 shows the significant decrease in ultimate impact speed with number of impacts.

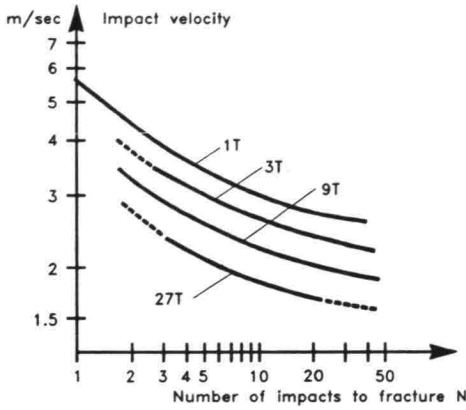


Fig. 2.10. Fatigue. Impact tests with prototype cubes. Silva (1983).

The above given Wöhler diagrams are all based on tests with zero mean stress. However, the fatigue effect is influenced by the mean stress level. The larger the mean stress the more pronounced is the fatigue if we assume constant stress fluctuation, $\Delta\sigma$. This is of importance because of the high static (mean) stress level in large slender types of armour units. The influence of the mean stress level is shown in Fig. 2.11 valid for pulsating and static load conditions.

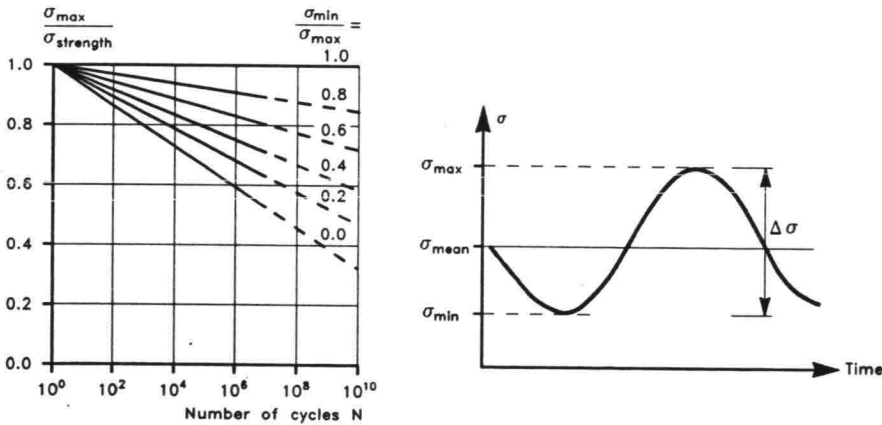


Fig. 2.11. Fatigue curves for unreinforced concrete (tensile and compressive stresses), RILEM 1984.

However, as long as σ_{max} is known it is not necessary to know σ_{mean} and σ_{min} in order to estimate the fatigue effect. A simple and slightly conservative method

would be to calculate the fatigue by setting $\Delta\sigma = \sigma_{max}$ (independent) on σ_{mean} and use the curves in Fig. 2.9. This will give almost the same result (within 5%) as if the fatigue was found from Fig. 2.11.

2.6.2 Reinforced concrete

Burcharth (1984) performed solid body impact fatigue tests with 200 kg Dolosse made of steel fibre reinforced concrete (2% by volume, 45 x 1 mm plain round fibres). Fig. 2.12 shows the results.

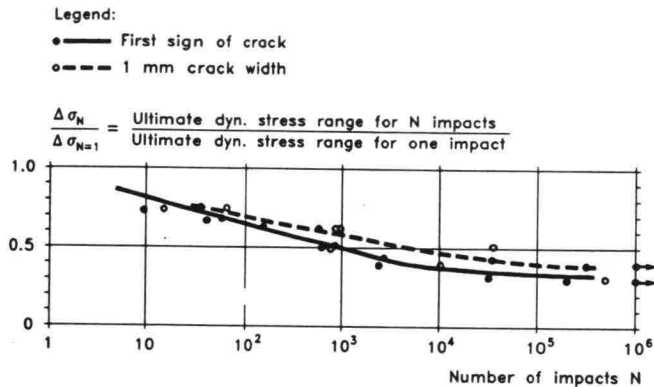


Fig. 2.12. *Fatigue. Solid body impact loading of rigidly supported steel fibre reinforced 200 kg Dolosse, causing flexural stresses with zero mean. Burcharth (1984).*

By comparing with Fig. 2.8 it is seen that the fatigue effect is somewhat reduced in the fibre reinforced units as it stabilizes at a stress range twice as big as for the unreinforced units for $N \geq 10^5$. A significant part of this better performance is probably due to the development of a more soft impact surface with a clear indentation.

As to fatigue effect in conventional bar reinforced concrete reference is made to the concrete literature.

2.6.3 Implementation of fatigue in the design process

The fatigue life is usually evaluated according to the *Palmgren - Minor accumulated damage theory* on the basis of an appropriate Wöhler diagram, e.g. Fig. 2.9.

The Palmgren - Minor rule expressing the cumulative damage ratio, D , reads

$$D = \sum_{i=1}^K \frac{\eta_i}{N_i} \leq 1 \quad (2.12)$$

where η_i is the number of cycles within the stress range interval i , N_i is the number

of cycles to failure at the same stress range derived from the Wöhler diagram, and K is the total number of stress range intervals. This implies that the number of stress cycles and the corresponding stress ranges throughout the lifetime of the structure must be estimated. This again means that the *long term sea state statistics* and the *relationship between a specific sea state and the related armour unit stresses* must be established.

Illustrative example

It is assumed that the stress history corresponding to a certain exceedence probability caused by the wave climate during structural life can be simplified to the stress range intervals $\Delta\sigma_{N_i}$ and related number of stress cycles η_i given below. Moreover, it is for simplicity assumed that the character of the stress variations corresponds to pulsating stresses and that the Wöhler diagram Fig. 2.9 for pulsating stresses is valid. The static tensile strength of the concrete is estimated to $S_T = 3 \text{ N/mm}^2$ which, for the given conditions, corresponds to the value of $\Delta\sigma_{N=1}$, in Fig. 2.9.

Stress history			Data from Wöhler diagram		
i	$\Delta\sigma_{N_i}(\text{N/mm}^2)$	η_i	$\Delta\sigma_{N_i}/\Delta\sigma_{N=1}$	N_i	$\frac{\eta_i}{N_i}$
1	2.4	50	0.8	10^3	0.05
2	2.1	$2 \cdot 10^3$	0.7	$2 \cdot 10^4$	0.10
3	1.8	10^5	0.6	$7 \cdot 10^5$	0.13
					$D = 0.28$

The fatigue effect then corresponds to an equivalent reduced tensile strength of $(1 - D)S_T = 0.72 \cdot 3 \simeq 2.2 \text{ N/mm}^2$. This value should then be used in the design of the armour units, for example when using the design diagrams in section 2.9.

It is important to notice that the accumulative effect of stress cycles presumes that the maximum tensile stress occurs in the same specific part of the material throughout the lifetime of the structure. This, however, will not be the case if the armour units are displaced during the structural life.

Consequently, if a chosen design damage level involves significant displacements it can be assumed that, most likely, the critical location of maximum tensile stresses in a unit will change during the displacement phase and will be different from the critical location of max tensile stresses when the unit is at rest at a later stage. This should be taken into account when assessing the stress history if overdesign should be avoided.

2.7 Ultimate impact velocities for concrete armour units

An indication of the relative strength of the various types of armour units can be given by the maximum impact velocity which a unit can resist without serious breakage.

No standard method exists for impact testing of the geometrically very different units and as a consequence no directly comparable results are available. The values of ultimate impact velocities given in Table 2.3 are rough estimates corresponding to solid body impact against a heavy rigid concrete base, causing breakage in terms of a mass loss of 20% or more.

Table 2.3. Approximate values of ultimate rigid body impact velocities for concrete armour units.

Armour unit	Impact velocity of centre of body (m/s)	Equivalent drop height of centre of body (m)
Cube, < 5 t	5 - 6	1.2 - 1.8
20 t	4 - 5	0.8 - 1.2
50 t	3 - 4	0.4 - 0.8
Tetrapod	2	0.2
Dolos, waist ratio 0.42	2	0.2
— , — — 0.32	1 - 1.5	0.05 - 0.12

If the armour units are not dropped on a hard rigid surface but on soil or a rock underlayer the ultimate impact velocities are significantly higher than those given in Table 2.3.

For evaluation of the placing technique during construction it is important to consider the ultimate impact velocities. The lowering speed of the crane at the moment of positioning of the units must be much lower than the figures given in Table 2.3.

When placing units underwater a heavy swell might impose rather large horizontal velocities of the unit when hanging from the crane. It is obvious from the figures in Table 2.3 that free fall dropping of concrete armour units by quick release from a crane or similar should be avoided because even small drop heights cause breakage. This is true also in case of underwater placement because the max free fall velocity underwater exceeds the limiting values given in the table except for very small massive types of units.

2.8 Thermal stresses

During the curing of the concrete the heat of hydration will increase the temperature. Because of the fairly low conductivity of concrete and because of the poor insulation of conventional formwork (e.g. steel shutter) a higher temperature will be reached in the centre part of the body than at the surface. The temperature difference will create different thermal expansion, but because of the coherence, the various parts of the body are not free to move and thus stresses are created. The bigger the distance from the centre to the surface the bigger the temperature difference and the stresses will be. The tensile stresses can easily exceed the very limited strength of the fresh young concrete thus causing formation of microcracks. Unfortunately, it is not possible to see thermal cracks because they will close at the surface due to the thermal contraction of the concrete when cooling off. Fig. 2.13 illustrates the formation of thermal stresses and cracks.

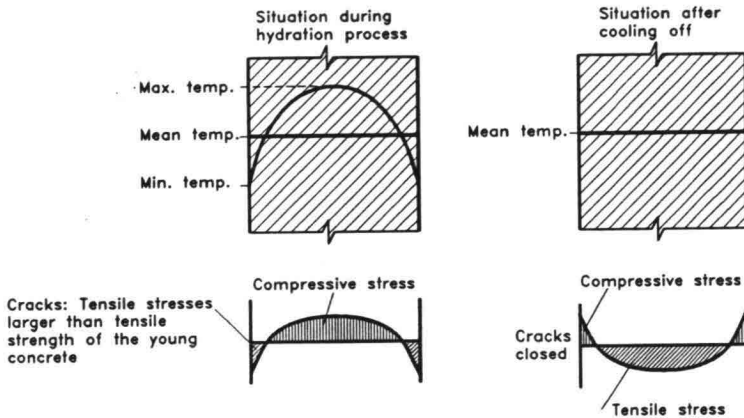


Fig. 2.13. Illustration of thermal stresses and related crack formation.

The process is very complicated and theoretically it can only be dealt with in an approximate manner, mainly because the description of creep and relaxation processes of the hardening concrete are not precise enough to avoid large uncertainties in the calculations. The calculations are performed by the use of special finite element computer programs for 3-dimensional bodies. The needed input is data on the concrete mix including the composition (type) of the cement, the concrete temperature when poured, the geometry of the units, the type of formwork (conductivity/insulation), the environmental climate (air temperature and wind velocities as function of time) and the cyclis time for removal of the formwork. The output of the calculations is the development of stresses and related crack formation as function of time. Fig. 2.14 shows an example of such a calculation for a 70t cube.

The cube will have no visible sign of weakness, but it will be fragile and brittle because the cracked regions at the surfaces and in the centre will have almost zero tensile strength and the non-cracked regions will be in tension. This means that

not only the strength but also the fatigue life and the resistance to deterioration will be reduced.

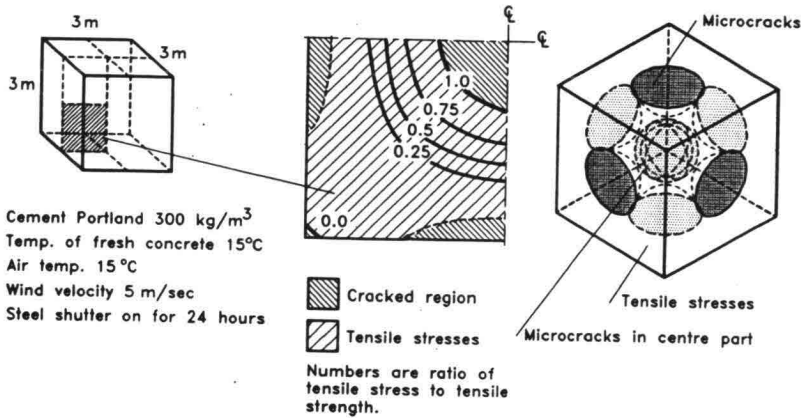


Fig. 2.14. Example of calculation of thermal stresses and cracked regions in a 70t cube 100 hours after casting. BKI-Institutet, Copenhagen and Burcharth, 1982.

There are several measures related to concrete technology for the prevention of damaging thermal stresses, but they all involve some drawbacks:

Measure to reduce thermal stresses	Drawback
Use of less cement	Reduced long term durability due to higher porosity. Higher production costs due to slower development of strength and longer cyclyus time for forms.
Use of low-heat cement or retarder	Higher production costs due to slower development of strength and longer cyclyus time for forms.
Cooling of water and aggregates	Higher production costs.
Use of insulation during part of the curing period	Higher production costs.

Insulation by means of a simple plastic cover was used by the author in 1981 related to trial casting of 90 t Antifer cubes applied for the emergency repair of the west breakwater at Sines in Portugal. The necessary number of days covering was determined by thermal stress calculations and presented in diagrams, Fig. 2.15.

Thermal stress calculations are complicated. However, a very important rule of thumb is that the temperature difference during curing should not exceed 20°C between any two points within the concrete element if thermal cracks should be avoided. The temperature difference is very easy and cheap to check by placing/casting copper-constantin thermo-wire (e.g. $2 \times 0.7 \text{ mm}^2$) in the concrete. The wire insulation must be removed at the tips which are placed at positions in the centre and near the surface of the units where the temperatures are maximum and minimum, respectively. Temperature readings can then be taken by connecting a pocket instrument to the free wire ends.

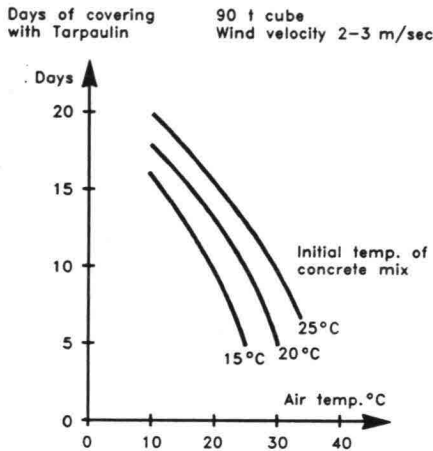


Fig. 2.15. Example of diagram to determine the minimum duration of insulation during curing for the prevention of thermal cracking. BKI-Institutet Copenhagen and Burcharth, 1982.

Another way of dealing with the thermal stress problem is to keep the effective dimensions of the armour units as small as possible. For cubes it can be done by making a hole as was done in the hot-climate Bosaso Harbour project in Somalia. Fig. 2.16 shows examples of the temperature development in 30 t blocks with and without a hole.

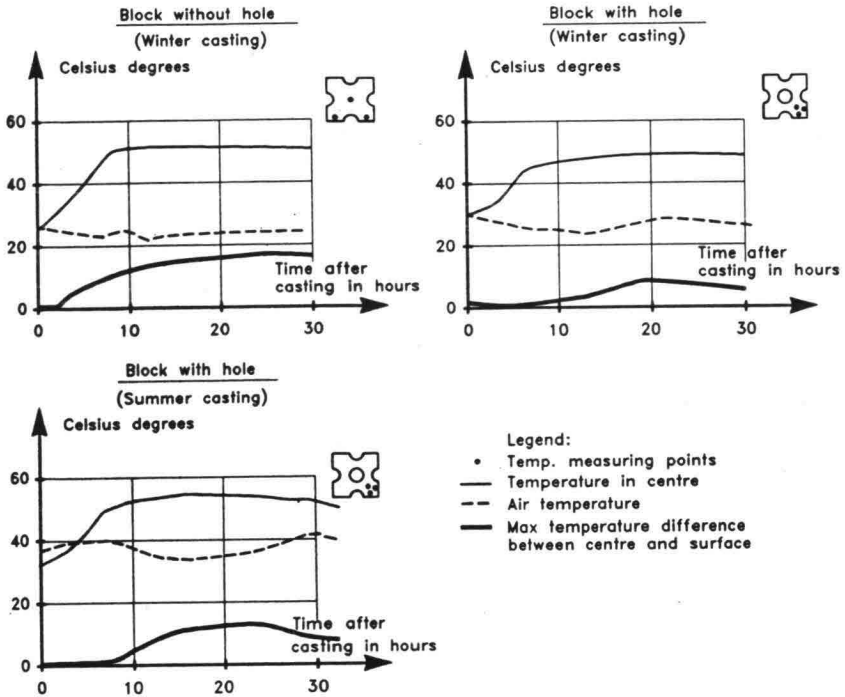


Fig. 2.16. Examples of temperature development during curing in 30 t modified cubes with and without a hole, Burcharth et al., 1991.

2.9 Design diagrams for Dolos of different waist ratios

The design diagrams in Figs. 2.18 A, B and C are based on model tests at Aalborg University (Burcharth et al. 1992) with instrumented Dolosse exposed to irregular waves. The diagrams contain design curves both for stress and displacement levels. The diagrams make it possible to choose a combination of mass and waist ratio which ensures both structural integrity and hydraulic stability. The amount of rocking is not given because this model is relevant only to breakage aspects which are dealt with specifically in the stress curves.

The test ranges are as follows:

- Waves : Irregular, breaking and non-breaking, head-on
- Slope : 1:1.5

Dolos : Waist ratios, $r = 0.32 - 0.42$. Random placement in two layers with packing density, $\varphi_{n=2} = 0.74$.

The hydraulic stability for Dolos armour on a slope 1:1.5 is given by (Burcharth and Liu):

$$N_s = \frac{H_{mo}}{\Delta Dn} = (47 - 72r) \varphi_{n=2} D^{1/3} N_z^{-0.1} \quad (2.13)$$

where

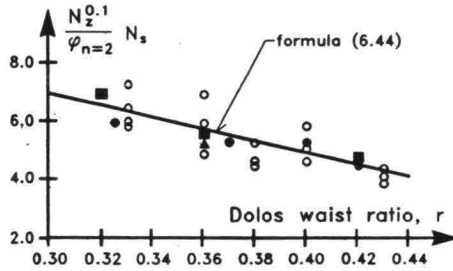
- H_{mo} : significant wave height in front of breakwater
- r : Dolos waist ratio
- $\varphi_{n=2}$: packing density for two layer armour
- D : relative number of units within levels SWL $\pm 6.5 Dn$ displaced one Dolos height h , or more (e.g. for 2% displacement $D = 0.02$)
- N_z : number of waves. For $N_z \geq 3000$ use $N_z = 3000$.

The eq. (2.13) is based on the model test results of Brorsen et al. (1974), Burcharth et al. (1986), Holtzhausen et al. (1991) and Burcharth et al. (1992). The formula (2.13) covers both breaking and non-breaking wave conditions, the limits given by the following parameters ranges

$$\begin{aligned} 0.32 &< r < 0.42 \\ 0.61 &< \varphi < 1 \\ 1\% &< D < 15\% \end{aligned}$$

The uncertainty of the formula is estimated to correspond to a coefficient of variation of approximately 0.22.

Fig. 2.17 gives an example corresponding to $D = 2\%$.



Legend:

Reference	$\varphi_{n=2}$	Repeated No	Duration (min.)	ξ_{mo}
▲ Brorsen et al. (1974)	1 (App.)	2	60	2.49–5.37
■ Burcharth et al. (1986)	0.61–0.7	5 or 15	20	3.04–4.49
● Holtzhausen et al. (1990)	1	3 or 8	60	2.91–7.6
● Burcharth et al. (1992)	0.74	20	5	3.23–11.7

$$\xi_{mo} = \tan \alpha (H_{mo} / \frac{2}{3} T_m)^{-0.5}, \quad \alpha = \text{slope angle}, \quad T_m = \text{mean wave period}$$

Fig. 2.17. Hydraulic stability of two layer randomly placed Dolos armour on a slope of 1 : 1.5. Damage level, $D = 2\%$ displaced units within levels $SWL \pm 6.5D_n$.

The design diagrams have been checked against observed behaviour of prototype Dolos breakwaters and good agreement was found.

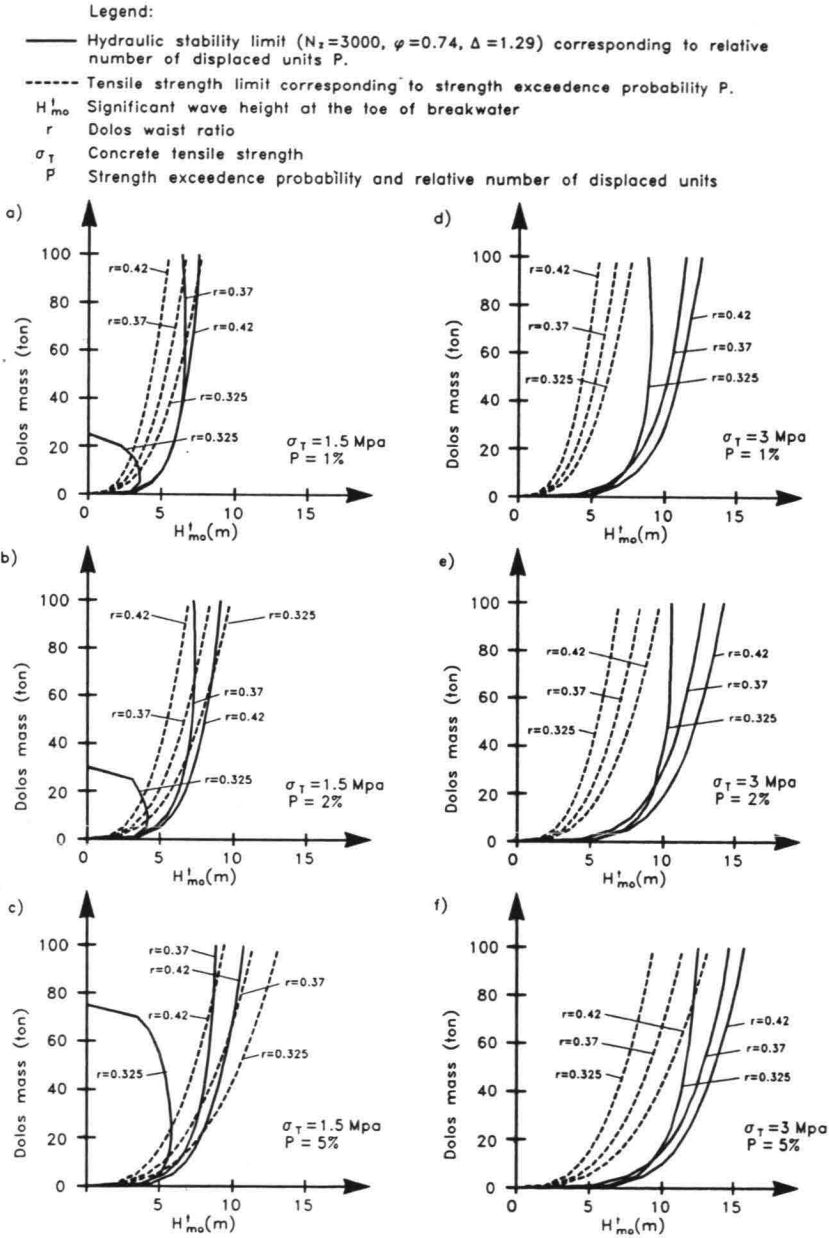


Fig. 2.18 A. Dolos design diagram.

Input: H_{mo}^t , Dolosmass, σ_T , P . Output: r

Legend:

- Hydraulic stability limit ($N_z=3000, \varphi=0.74, \Delta=1.29$) corresponding to relative number of displaced units P .
- - - - Tensile strength limit corresponding to strength exceedance probability P .
- H_{mo}^+ Significant wave height at the toe of breakwater
- r Dolos waist ratio
- σ_T Concrete tensile strength
- P Strength exceedance probability and relative number of displaced units

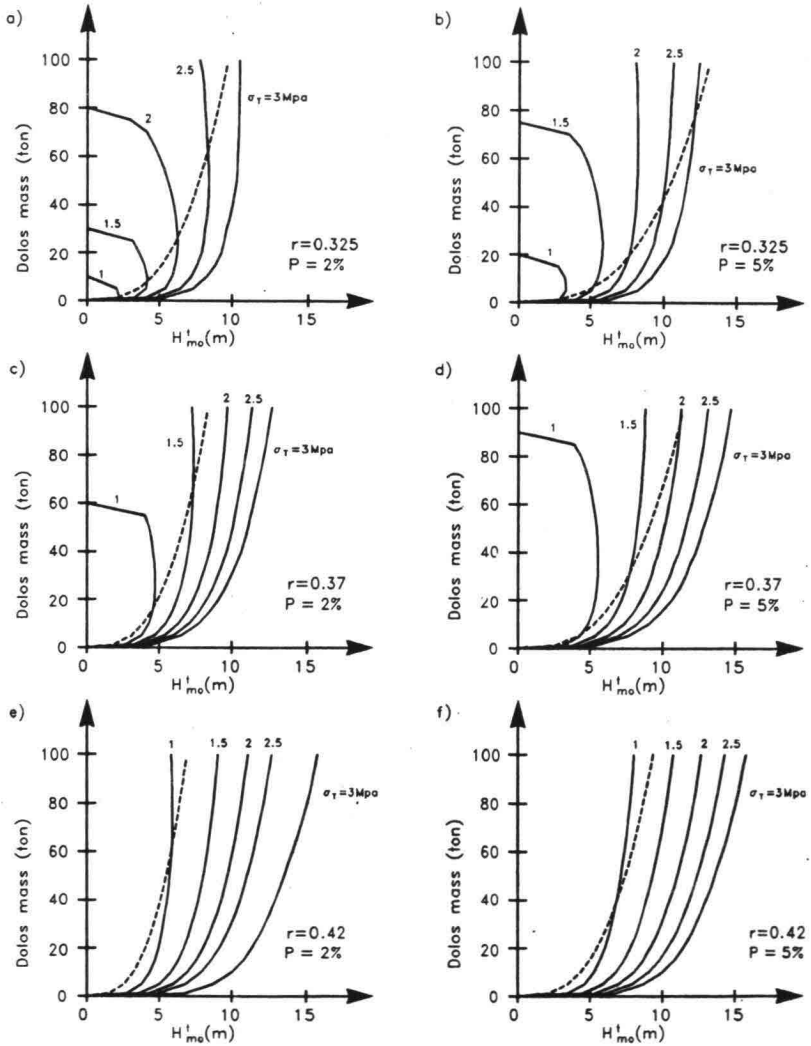


Fig. 2.18 B. Dolos design diagram.

Input: H_{mo}^+ , Dolosmass, r , P . Output: σ_T

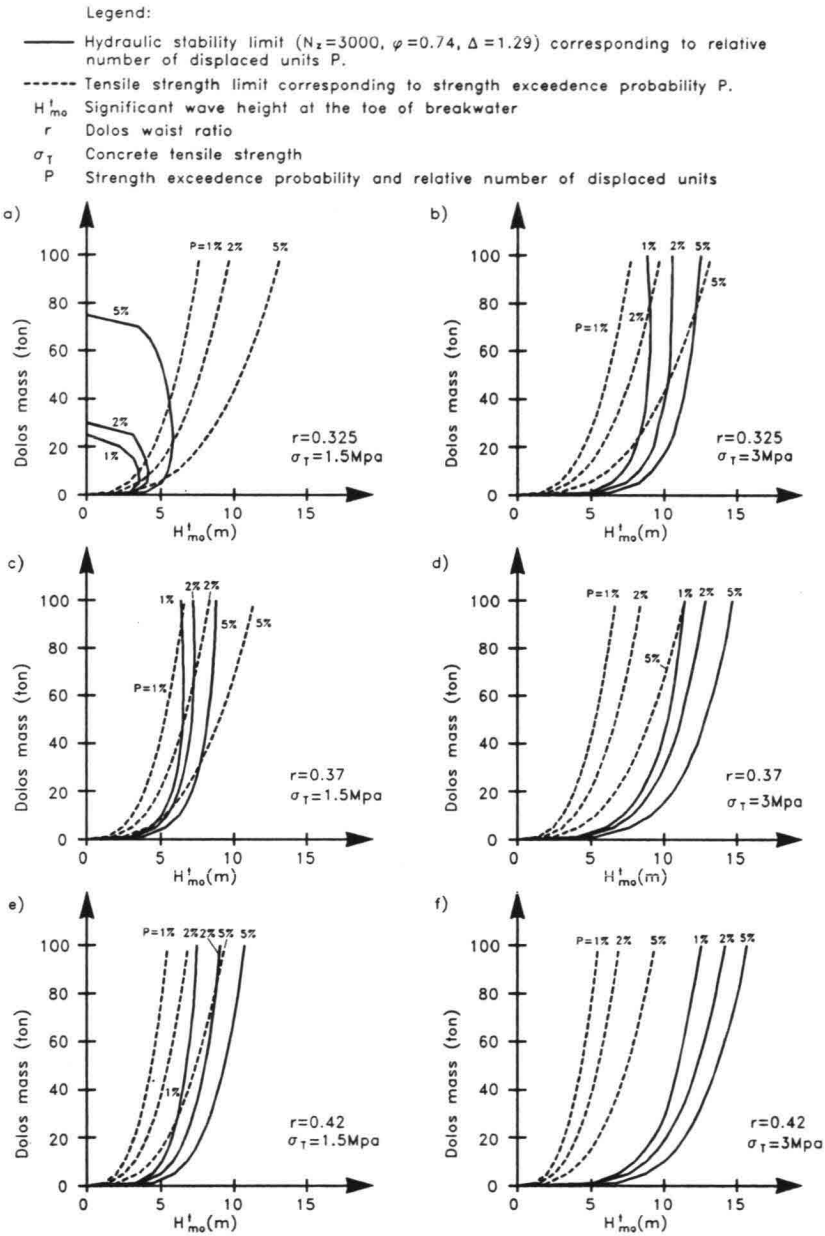


Fig. 2.18 C. Dolos design diagram.
 Input: H_{mo}^t , Dolosmass, r , σ_T . Output: P

æ

3. References

- Brorsen, M. Burcharth, H.F. and Larsen, T. , 1974. *Stability of Dolos Slopes*. Proc. 14th Coastal Engineering Conference, Copenhagen.
- Burcharth, H.F. , 1981. *Full-scale dynamic testing of dolosse to destruction*. Coastal Engineering, Vol.4, 1981.
- Burcharth, H.F. , 1983. *Comments on the paper by G.W.Timco titled "On the structural integrity of dolos units under dynamic loading conditions"*. Coastal Engineering, Vol.7, No.1, Feb.1983.
- Burcharth, H.F. , 1984. *Fatigue in breakwater armour units*. Proceeding of the 19th International Conference on Coastal Engineering, Houston, Texas, Sept. 1984.
- Burcharth, H.F. and Brejnegaard-Nielsen, T. , 1986. *The influence of waist thickness of dolosse on the hydraulic stability of dolos armour*. Proceeding of the 20th International Conference on Coastal Engineering, Taipei, Taiwan, Nov. 1986.
- Burcharth, H.F. and Howell, G.L. , 1988. *On methods of establishing design diagrams for structural integrity of slender complex types of breakwater armour units*. Seminaire International Entretien des Infrastructures Maritimes. Casablanca, Marocco, 1988.
- Burcharth, H.F. and Liu Z. , 1990. *A general discussion of problems related to the determination of concrete armour unit stresses including specific results related to static and dynamic stresses in Dolosse*. Proc. Seminar Stresses in Concrete Armor Units, ASCE, Vicksburg, U.S.A., 1990.
- Burcharth, H.F., Howell, G.L. and Liu Z. , 1991. *On the determination of concrete armour unit stresses including specific results related to Dolosse*. Coastal Engineering 15, 1991.
- Burcharth, H.F. and Liu, Z. , 1992. *Design Dolos armour units*. To be published in Proc. 23th Coastal Engineering Conference, Venice, Italy, 1992.
- Bürger, W.W., Qumeraei, H. and Partensky, H.W. (1990) , 1990. *Impact Strain Investigations on Tetrapods: Results of Dry and Hydraulic Tests*. Proc. Seminar Stresses in Concrete Armor Units, ASCE, Vicksburg, U.S.A., 1990.
- CIRIA, CUR , 1991. *Manual on the use of rock in coastal and shoreline engineering*.
- DHL , 1980. Hydro Delft No 56, March 1980, Delft Hydraulic Laboratory, Holland, 1980.
- Fagerlund, G. and Larsson, B. , 1979. *Betongs slaghalfasthed (in Swedish)*. Swedish Cement and Concrete Research Institute at the Institute of Technology, Stockholm, 1979.

- Holtzhausen, A.H., Zwamborn, J.A. , (1990). *Stability of Dolosse with different waist thickness for irregular waves*. Proc. 22nd ICCE, Delft, Holland, 1990.
- Howell, G.L. , 1990. *Stresses in Dolos armour units due to waves*. Proc. Seminar Stresses in Concrete Armor Units, ASCE, Vicksburg, U.S.A., 1990.
- Ligteringen, H., Altink, H. and van Orschot, J.H. , 1990. *Strength of Concrete Armour Units: A Joint Industry Research*. Proc. Seminar Stresses in Concrete Armor Units, ASCE, Vicksburg, U.S.A., 1990.
- Markle, D.G. , 1990. *Crescent City Instrumented Model Dolos Study*. Proc. Seminar Stresses in Concrete Armor Units, ASCE, Vicksburg, U.S.A., 1990
- RILEM , 1984. *Report by RILEM Technical Committee 36-RDL on Long-Term Random Dynamic Loading of Concrete Structures*. RILEM, Materials and Structures, Vol. 17, No. 97, January/February, 1984.
- Sandstrom, A. , 1974. *Wave forces on blocks of rubble mound breakwaters*. Hydraulic Lab. Bulletins No. 83, Royal Institute of Technology, Stockholm, Sweden, 1974.
- Scott, R.D., Turcke, D.J. and Baird, W.F. , 1986. *A unique instrumentation scheme for measuring loads in model dolos units*. Proceeding of the 20th International Conference on Coastal Engineering, Taipei, Taiwan, Nov. 1986.
- Silva, M.A.G. , 1983. *On the mechanical strength of cubic armour blocks*. Proc. Coastal Structures '83, Arlington, Virginia.
- Tait, R.B. and Mills, R.D.W.B. , 1980. *An investigation into the material limitations of breakwater Dolosse*. ECOR newsletter No. 12, 1980
- Tepfers, R. and Kutti, T. , 1979. *Fatigue strength of plain ordinary and lightweight concrete*. ACI Journal, May, 1979.
- Timco, G.W. , 1981. *The development, properties and production of strength-reduced model armour units*. Lab. Tech. Report, Nov. 1981. Hydraulics Lab. Ottawa, NRC, Canada.
- Timco, G.W., Mansard, E.P.D. , 1983. *On the interpretation of rubble-mound breakwater tests*. Proc. Coastal Structures '83, Arlington, Virginia.
- van der Meer, J.W. and Heydra, G. , 1991. *Rocking armour units: Number, location and impact velocity*. Coastal Engineering 15, 21-39.
- Zielinski, A.J., Reinhardt, H.W. and Körmeling, H.A. , 1981. *Experiments on concrete under repeated uniaxial impact tensile loading*. RILEM, Materials and Structures, Vol. 14, No. 81, 1981.
- Zwamborn, J.A. and D. Phelp, D. , 1990. *Structural Tests on Dolosse*. Proc. Seminar Stresses in Concrete Armor Units, ASCE, Vicksburg, U.S.A., 1990